www.amlett.com, www.vbripress.com/aml, DOI: 10.5185/amlett.2015.5737 Published online by the VBRI press in 2015

Sequentially reduced biogenic silver-gold nanoparticles with enhanced antimicrobial potential over silver and gold monometallic nanoparticles

Dipali Nagaonkar, Mahendra Rai*

Nanobiotechnology Lab., Department of Biotechnology, S.G.B. Amravati University, Amravati 444 602, Maharashtra, India

*Corresponding author. Tel: (+91) 814662378; E-mail: mkrai123@rediffmail.com

Received: 15 October 2014, Revised: 13 December 2014 and Accepted: 24 December 2014

ABSTRACT

Bimetallic nanoparticles have emerged up as advanced nanomaterials due to the synergism between two metallic nanoparticles in core-shell or alloy arrangement. Moreover, bioinspired synthesis of nanoparticles is an evergreen approach of nanobiosciences. In this experiment, we have fabricated silver, gold and silver $_{(core)}$ - gold $_{(shell)}$ bimetallic nanoparticles using leaf extract of *Catharanthus roseus* Linn. by sequential reduction technique. The sequentially reduced silver-gold nanoparticles in core-shell arrangement were detected by shift in the surface plasmon resonance of nanoparticles from 423 nm to 526 nm with the aid of UV-Visible spectrophotometer. Nanoparticle tracking analysis confirmed the mean particle size for all the nanoparticles within the range 11 to 65 nm. X-Ray diffraction analysis revealed Bragg's reflections denoting face cubic centered crystalline nature of all the synthesized nanoparticles. Transmission electron microscopy showed that silver and silver-gold nanoparticles are quite polydispersed and spherical in shape while anisotropic Au nanoparticles were also observed. These phytofabricated Ag-Au nanoparticles have been evaluated with enhanced antibacterial and anticandidal potential over their monometallic counterparts with particular reference to some pathogenic bacteria and *Candida* sp. The maximum lethality of bimetallic nanoparticles was observed for *Escherichia coli* followed by *Pseudomonas aeruginosa*, while *Candida parapsilosis* was found to be the least susceptible organism for the silver-gold nanoparticles. Copyright © 2015 VBRI press.

Keywords: Bimetallic nanoparticles; *Catharanthus roseus* Linn.; core-shell arrangement; phytofabrication; sequential reduction.

Dipali Nagaonkar has graduated from Mumbai University (2009) and obtained her M.Sc. degree in 2011 in Botany. She is currently working under the supervision of Prof. Mahendra Rai at Department of Biotechnology, S.G.B. Amravati University for her doctoral studies. She received DST-INSPIRE fellowship in 2013. Her research area of interest is development of mono and bimetallic as well as polymeric nanomaterials for applications in drug delivery and as antimicrobial agents.

Mahendra Rai is a Professor and Head at Department of Biotechnology, S.G.B. Amravati University at Amravati, Maharashtra, India. His area of expertise includes microbial biotechnology and nanobiotechnology. His present research interests are nanobiotechnology in medicine and agriculture, in particular the use of metallic nanoparticles as new generation of antimicrobials. He has published more than 250 research papers in India and abroad. In addition, he has edited/authored more than 31 books and 6 patents.

Introduction

During the recent years, nanotechnology has experienced revolutionary shift from monometallic to multimetallic nanostructures with advanced physicochemical, optical and magnetic properties **[1]**. Structural changes made on the surface of nanoparticles by alloying or arranging 2 or more metals in core-shell arrangement play crucial role in properties of multimetallic nanoparticles. Bimetallic nanoparticles with advanced physicochemical properties have started up a new era in the field of various applications such as electrocatalysis **[2]**, nanobiosensors **[3]**, drug delivery, *in vivo* imaging **[4]**, etc. Owing to their high surface area and synergism between two metal variables at the nanoscale level, gold-based core-shell nanostructures are found to possess high catalytic potential for many important oxidation reactions including hydrogen oxidation, methanol oxidation and oxygen reduction reaction **[5]** as well as electrocatalysts for fuel cell

applications **[6]**, etc. as compared to their monometallic counterparts.

The synthesis strategy for bimetallic nanoparticles mainly involves simultaneous or successive reduction of two metal components resulting into nanoparticles in either core–shell or alloy arrangement. Unlike the simultaneous or co-reduction method, successive or sequential reduction method (seed mediated growth technique) yields bimetallic nanoparticles in predetermined core-shell arrangement rather than alloy particles **[7]**. Sequential reduction method for bimetallic nanoparticles relies upon reduction of shell metal component over pre-formed core metal component, referred to as seed. However, along with preparation conditions, the structure of bimetallic combinations depends mainly upon the nobility, miscibility as well as redox potential of metal elements **[7]**. Similarly, precise control over nucleation and transition phases of ions to nanoparticles is required for formation of bimetallic nanostructures **[8]**. Now-a-days, various physical and chemical synthetic techniques are being employed for the fabrication of bimetallic nanoparticles including sol-gel method, sonochemical method **[9]**, microemulsion technique **[10]**, aerosol technology **[11]**, etc. For instance, Zhang et al. (2013) has reported hollow Ag-Au bimetallic nanoparticles by reducing gold ions over the silver seeded nanoparticles in galvanic replacement reaction **[12]**. However, all these toxic solvent dependent methods are considered to be expensive, time consuming as well as hazardous from the environmental point of view.

Bioinspired synthesis of bimetallic nanoparticles appears to be reliable, non toxic and sustainable approach towards development of advanced class of nanomaterials with superior catalytic properties. Biosynthesis of bimetallic nanoparticles by algae, fungi and higher plants as reducing agents have been gaining immense attention as a viable alternative for the hazardous physicochemical techniques. For instance, leaves of *Anacardium occidentale* were used by Sheny and co-workers (2011) for phytofabrication of Au-Ag core-shell and alloy nanoparticles **[13]**. Aqueous extract of sago pondweed, *Potamogeton pectinatus* was found to be an effective algal system for the synthesis of polydispersed Au-Ag bimetallic nanostructures **[14]**. Fungal system *Neurospora crassa* was employed by Castro-Longoria et al. (2011) for the mycosynthesis of bimetallic Au-Ag nanoparticles **[15]**. So far, all these researchers have employed simultaneous reduction method for the preparation of bimetallic nanoparticles of gold-silver in core-shell arrangement. However, biogenic transformation of two or more metals into core-shell nanoparticles by sequential reduction method has not been reported yet.

The phytosynthesized core-shell nanoparticles with combinations of silver and gold are promising materials in various biomedical fields due to their antibacterial **[16]** and anticancer **[17]** properties. It is now a well established fact that silver nanoparticles (AgNPs) exert very strong antifungal, antiviral, antiprotozoal and bactericidal activity against both Gram positive and Gram negative bacteria as well as multiresistant strains **[18-20]**. Though, gold nanoparticles (AuNPs) do not show significant antimicrobial effect **[16]**, very few authors have reported antibacterial activity of gold nanoparticles against Gram-positive and Gram-negative bacteria **[21]**. Therefore, it is of interest to some researchers whether AuNPs in synergy, can influence bioactivity of other antimicrobial nanoparticles as they are known to possess strong catalytic properties.

To the best of our knowledge, this is the first report for the synthesis of Ag, Au and Ag-AuNPs using seed mediated growth technique or sequential reduction reaction. In this experiment, we aim at *Catharanthus roseus* leaves mediated green synthesis and characterization of silver, gold and silver (core)-gold (shell) bimetallic nanoparticles by sequential reduction method. Further, these phytosynthesized bimetallic nanoparticles were evaluated for synergistic effect of silver and gold nanoparticles against some pathogenic bacteria and *Candida* sp.

Experimental

Materials

Silver nitrate ($AgNO_3$) and Chloro auric acid ($HAuCl_4$) (purity 99.95%) were received from Hi media, Mumbai, India and were used as received.

Preparation of leaf extract

The mature leaves of *C. roseus* Linn. were collected from premises of Department of Biotechnology, S.G.B. Amravati University, Amravati, Maharashtra, India. The leaf extract of *C. roseus* was prepared by boiling 8 gm of leaves in 100 ml of distilled water. The extract was filtered by filter paper and centrifuged at 4000 rpm for 30 min. The filtrate was used for the synthesis of silver, gold and bimetallic silver-gold nanoparticles.

Synthesis of AgNPs, AuNPs and Ag-Au bimetallic nanoparticles

For phytosynthesis of AgNPs and AuNPs, 10 ml of aliquot of leaf extract was incubated with 90 ml of 10^{-3} M $AgNO_3$ and $HAuCl_4$ ion solutions. Both reaction mixtures were allowed to react at room temperature for 30 min and the change in colour of the solution was observed. For synthesis of Ag-AuNPs by two step sequential reduction method, 10 ml leaf filtrate was allowed to react with 90 ml of 10^{-3} M $AgNO_3$ at room temperature. After 30 min, on confirmation of colour change from colourless to ruby -red, 1 ml of 10^{-2} M gold chloride ion solution was introduced into the reaction mixture. The reaction mixture was again incubated at room temperature and observed up to the development of final colour.

UV-visible absorbance spectroscopy

The bioreduction of Ag^+, Au^+ and Ag^+-Au^+ to Ag^0, Au^0 and Ag^0-Au^0 was confirmed by subjecting diluted aliquots of the silver, gold and silver-gold bimetallic nanoparticles to UV-Visible spectrophotometer (Model- Shimadzu UV-1700, Japan) in the range of 300-800 nm.

Nanoparticle tracking analysis (NTA)

Nanoparticle tracking analysis was performed through Nanosight LM 20 (UK) to measure the size of the nanoparticles. For this, 5 µl of the nanoparticle samples were diluted with 2 ml of distilled water and injected onto

the sample chamber and observed through camera fixed with the instrument.

Zetasizer analysis

Zetasizer analysis was carried out to determine zeta potential and polydispersity index of biosynthesized nanoparticles. 30 µl of nanoparticle solution diluted with 2 ml of distilled water were taken into zeta dip cell and measured by Malvern Zetasizer 90 (ZS 90, USA).

X-ray diffraction (XRD) analysis

XRD measurements of purified silver, gold and silver-gold core-shell nanoparticle solutions casted onto the glass slide were carried out using Phillips PW 1830 instrument at 2θ angle in the range 20° to 80°.

Fourier transform infrared spectroscopy (FTIR) studies

For determination of surface functionalities and metabolites of leaf extract responsible for reduction of ions and capping of nanoparticles, FTIR studies were performed on Perkin-Elmer FTIR-1600, USA. Sample was prepared by mixing purified nanoparticles with 10 mg of potassium bromide powder and dried to remove the moisture content.

Transmission electron microscopy (TEM) and selected area electron diffraction (SAED) measurements

Size and morphological studies of phytosynthesized silver, gold and silver-gold nanoparticles were performed with the aid of TEM and SAED on instrument PHILIPS model CM 200. For TEM analysis, samples were prepared by drop coating of Ag, Au and Ag-Au nanoparticles suspension on conventional carbon coated copper grids.

Antibacterial and anticandidal assay of Ag, Au and Ag-AuNPs

The antibacterial and anticandidal activities of Ag, Au and Ag-AuNPs against some pathogenic bacteria including *Staphylococcus aureus* (ATCC-33591), *Pseudomonas aeruginosa* (MTCC-4676) and *Escherichia coli* (ATCC-14948), and *Candida* sp. including *C. utilis* (NCIM-30515), *C. parapsilosis* (NCIM-3323) and *C. guilliermondii* (NCIM-3110) were assayed by disc-diffusion method and evaluated for minimum inhibitory concentrations (MIC).

Disc-diffusion assay

The standard chloramphenicol and ketoconazole loaded antibiotic discs were purchased from Hi-Media, Mumbai, India. Kierby-Bauer disc diffusion assay was performed against *S. aureus*, *P. aeruginosa* and *E. coli* on Muller–Hinton agar plates. A single colony forming unit of individual test organism was grown overnight in Muller–Hinton broth at 37°C. 100 µl of inoculum (approx. concentration 10^5 CFU/ml) of each bacterium was streaked onto the agar plates and then standard and prepared discs impregnated with Ag-NPs, AuNPs, Ag-AuNPs, and the individual combinations of AuNPs and Ag-AuNPs with standard antibiotic discs were placed onto the agar surface. The prepared disc with leaf extract was placed as a control. Upon incubation at 37°C for 24 hrs, the zones of inhibition were measured in terms of mm.

Similarly, Sabouraud dextrose agar plates were inoculated with 100 µl of preformed inocula (concentration 10^5 CFU/ml) of *C. guilliermondii*, *C. parapsilosis* and *C. utilis*. The combinations of discs as mentioned above were placed onto the agar surface and incubated at 37°C for 24 hrs followed by measurement of the zones of inhibition.

Determination of MIC of silver and silver-gold nanoparticles

Broth dilution method was used to determine MIC of AgNPs and Ag-AuNPs against bacteria and *Candida* sp. The inocula from the broth containing 1×10^8 CFU/ml was taken into wells of microtiter plate accordingly, to make the final cell number up to 1×10^6. To these 8 wells, Ag-NPs and Ag-AuNPs of concentration 2, 4, 6, 8, 10, 20, 40 and 60 µg ml^{-1} against bacteria and 5, 10, 15, 20, 25, 30, 40 and 50 µg ml^{-1} against *Candida* sp. were added. According to this concentration, the stock solution of broth was added to the wells containing test organisms. For the visual observation, the microtiter plates were incubated at 37°C for 24 hrs. On completion of incubation period, 40 µl of tetrazolium salt prepared in distilled water was added to each microwell and observed for the colour change.

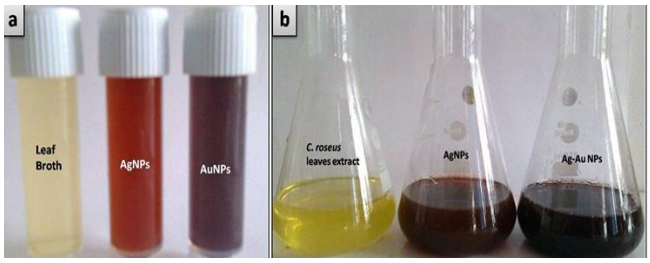

Fig. 1. Showing colour changes for (a) AgNPs (ruby-red) and AuNPs (dark -purple); (b) Ag-AuNPs (reddish- brown to dark- purple).

Results and discussion

UV-Visible spectrophotometry

The rapid reduction of silver and gold ions into nanoparticles were primarily detected by change in colour of the reaction mixture from transparent- yellow to ruby -red and dark -purple for silver and gold nanoparticles respectively as shown in **Fig. 1 a**. The transformation of metal ions into nanoparticles was further confirmed by UV-Visible spectra (**Fig. 2 a** and **b)** as a function of time with strong absorbance peaks at 424 nm and 546 nm reported to be specific for AgNPs and AuNPs respectively. In case of Ag-Au bimetallic nanoparticles formed by sequential reduction, core-shell arrangement of the nanoparticles was detected by shift of absorbance peak of nanoparticulate seed to absorbance peak of newly formed nanoshell. Herein, the nano silver seed was recorded with absorbance peak at 423 nm, which upon introduction with gold ions, was observed to be shifted to 536 nm, characteristic of AuNPs (**Fig. 2c**). The complete disappearance or replacement of former absorbance peak of core component by absorbance peak of shell metal component strongly indicates reduction of later onto the surface of

nanoparticulate seed and formation of chemical environment over the seed surface. Increase in intensity of absorbance of SPR over the period of time is may be due to the increase in concentration of nanoparticles by continuous reduction of free ions present in the suspension the nanoparticles **[22]**. Upon introduction of the aqueous gold ions with preformed solution of silver nanoparticle, the silver nanoparticle solution changed rapidly from reddish-brown to dark purple within a minute (**Fig. 1b**), suggesting towards rapid synthesis of smaller-sized silver-gold bimetallic nanoparticles.

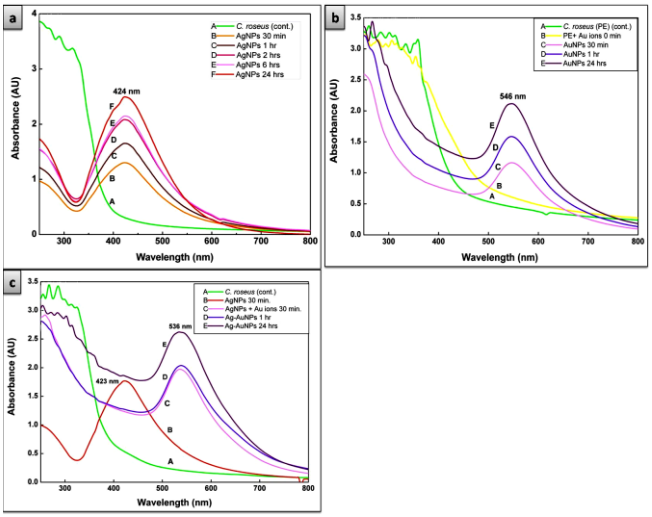

Fig. 2. UV-Visible absorbance spectra recorded as a function of time for (a) silver (b) gold and (c) silver-gold nanoparticles synthesized by leaf extract of *C. roseus*.

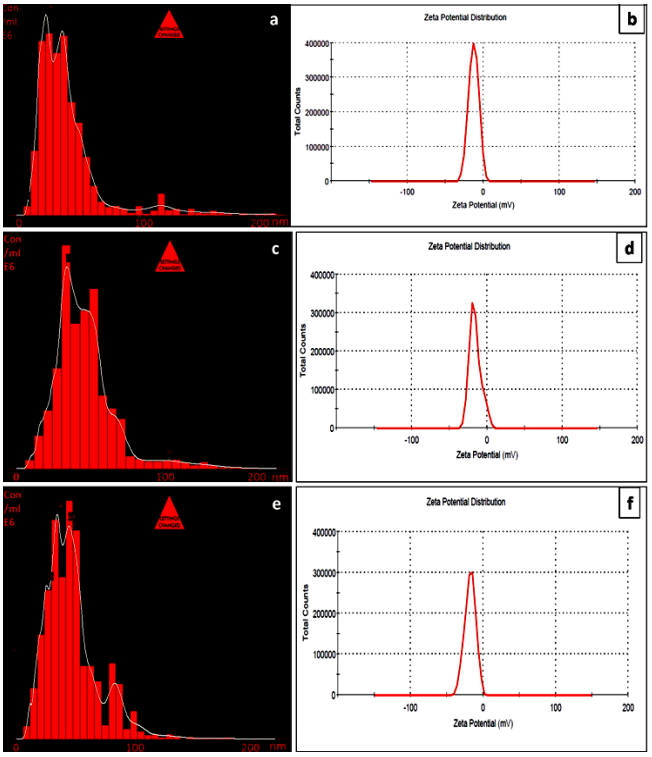

Fig. 3. NTA Size distribution histograms of (a) AgNPs, (c) AuNPs, (e) Ag-AuNPs and Zeta potential analysis of (b) AgNPs, (d) AuNPs, (f) Ag-AuNPs.

Nanoparticle tracking analysis

Nanoparticle tracking analysis divulges size of nanoparicles by tracking the brownian motion of particles freely suspended in colloidal solution. Mean size of nanoparticles was calculated by tracking minimum of 1000 nanoparticles active in brownian motion. NTA revealed quite polydispersed population of Ag, Au and Ag-Au nanoparticles of mean size 44±35 nm, 46±23 nm and 48±23 nm respectively. The size histograms of AgNPs, AuNPs and Ag-AuNPs are evident from **Fig. 3 (a, c** and **e)** respectively.

Zeta sizer analysis

Zeta sizer analyses of all the three kinds of phytosynthesized nanoparticles were performed to determine zeta potential and polydispersity index (PDI). Negative zeta potential denoting negative surface charge was observed for AgNPs (-12.9 mV) (**Fig. 3b**), AuNPs (-15.8 mV) (**Fig. 3d**) and Ag-AuNPs (-18.0 mV) (**Fig. 3f**). Nanoparticles found to be highly stable over a considerable period of time, which can be attributed to capping layer derived from metabolites present in the leaf extract. Polydispersity index was calculated as 0.75 for AgNPs, 0.81 for AuNPs and 1.0 for Ag-AuNPs revealing heterogenecity of the nanoparticle populations.

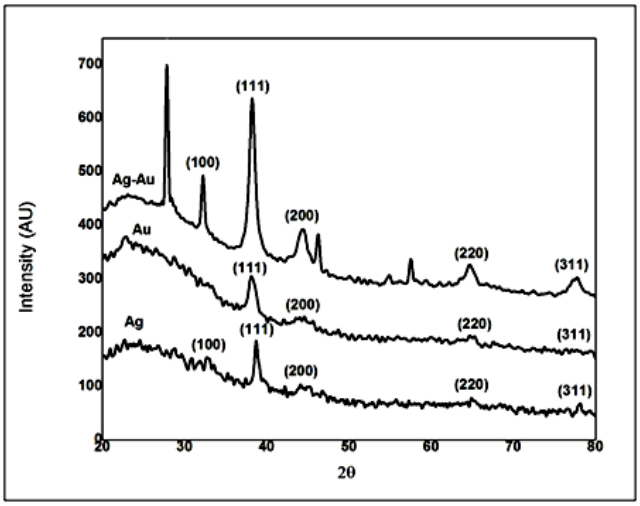

Fig. 4. X-Ray diffraction patterns of AgNPs, AuNPs and Ag-AuNPs.

X-Ray diffraction studies

Crystalline nature of nanoparticles was determined by Bragg's reflection peaks evident from X-Ray diffraction pattern (**Fig. 4**). The broadening of peaks clearly reveals formation of particles within the nanometer range. For AgNPs, Bragg's reflections peaks at 2θ value of 32.74º, 38.57º, 44.17º, 65.07 º and 78.02 º corresponds to (100), (111), (200), (220) and (311) lattice planes respectively, indicates face cubic centered (fcc) crystalline nature of nanoparticles (JCPDS file No. 04-0783). In case of AuNPs, the fcc nature of crystalline gold nanoparticles was revealed by Bragg's reflections peaks appeared at 38.12º (111), 44.46º (200), 64.76º (220) and 78º (311) lattice planes (JCPDS file No.04-0784). XRD pattern of Ag-Au bimetallic nanoparticles shows intense peak at 38.2 º

corresponds to (111) plane as compared to other peaks, 32.1º, 44.3º, 64.6º and 77.6º indexed to (100) (200) (220) and (311) respectively. Unidentified peaks in all the XRD patterns including a sharp peak at 28.7º appeared for Ag-AuNPs can be attributed to the crystalline nature of capping proteins present over the surface of nanoparticles **[22]**.

Fourier transform infrared spectroscopy studies

FTIR spectroscopic analysis was carried out to study chemistry of small molecules adsorbed on the surface of nanoparticles. As described in experimental section, centrifuged and purified nanoparticle solutions were used for FTIR analysis, which ensures elimination of interference from free biomass. FTIR spectra of purified silver, gold and silver-gold nanoparticles were analyzed and compared with spectra of leaf extract as control. The main peaks that appear in spectra recorded for leaf extract were ~1634, ~1501, ~1462, ~1387, ~1109, ~603 and ~550 cm^{-1} (**Fig. 5a**). The band around ~1634 cm^{-1} can be ascribed to N-H bending of 1º amines or -C=C- or aromatic groups **[23]**. The weak absorbance peak appeared at ~1501 cm^{-1} can be assigned to N-O asymmetric stretching of nitro compounds most probably the alkaloids present in the leaf extract. The minor peak at ~1462 cm^{-1} is associated with C-H bending of functional group alkanes. The major peak at ~1387 cm^{-1} can be ascribed to geminal methyls **[24]**. Another major peak at ~1109 cm^{-1} can be attributed to -C-O groups of polyols such as flavones, triterpenoids and polysaccharides. The complete disappearance of band at ~1109 cm^{-1} from spectra recorded for silver and gold nanoparticles suggest polyols as responsible bioconstituents for bioreduction of metal ions into nanoparticles. The minor peaks appearing at ~603 cm^{-1} and ~550 cm^{-1} can be assigned to C-Cl/C-Br and C-Cl stretching of alkyl halides respectively.

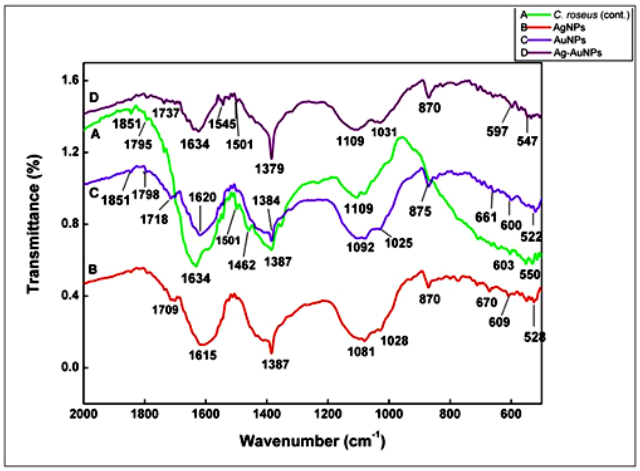

Fig. 5. FTIR spectra recorded for **(a)** leaf extract of *C. roseus*, **(b)** AgNPs, **(c)** AuNPs and **(d)** Ag-AuNPs

The FTIR spectra recorded for AgNPs (**Fig. 5b**) shows major peaks at ~1615 (-C=-C or aromatic groups) **[23]**, ~1387 (geminyl methyls), ~1081 cm^{-1} (C=O stretchings of alcohols, carboxylic acids, esters and ethers) **[25]**, while some minor peaks appear at ~1709 (C-C stretch of alkenes), ~1028 (C-N stretchings of aliphatic amines), ~870 (C-Cl stretch of alkyl halides), ~670 (C-H "oop" of aromatic compound), ~609 (C-Cl/C-Br stretchings of alkyl halides) and ~528 cm^{-1} (C-Br stretchings of alkyl halides). In case of AuNPs (**Fig. 5c**), minor peaks at ~1798 and ~1718 cm^{-1} represents C=O stretching of carbonyl group in ketones, aldehydes, and carboxylic acids **[26, 23]**. The major peaks appeared at ~1620 cm^{-1} and ~1384 cm^{-1} can be assigned to stretching vibrations of -C=C- or aromatic groups **[23]** and geminal methyls respectively. Another major peak recorded at ~1081 cm^{-1} represents C=O stretchings of alcohols, carboxylic acids, esters and ethers **[25]**. The minor peak at ~1025 cm^{-1} is assigned to C-N stretch of aliphatic amines. The absorption peak at ~875 cm^{-1} is ascribed to C-H "oop" of aromatic groups, while other minor peaks at ~661, ~600 and ~522 cm^{-1} represents C-Cl or C-Br stretch of alkyl halides.

The FTIR spectra of Ag-Au bimetallic nanoparticles (**Fig. 5d**) was recorded with some major peaks at ~1634, ~1379 and ~ 1109 cm^{-1} corresponds to amide bond I of proteins, geminal methyls and polyols including flavones, triterpenoids and polysaccharides as predominant surface capping functionalities respectively. The minor peak at ~1545cm^{-1} can be due to the amide II band of peptide linkages. The other minor peaks were observed at ~1737 (C=O stretching of carbonyl group in ketones, aldehydes and carboxylic acid), ~1501 (C-C stretching of aromatic compounds), ~1031 (C-O stretching of alcohols, carboxylic acids, esters and ethers), ~870 (C-H "oop" aromatics), ~597 and ~547 cm^{-1} (C-Cl and C-Br stretch of alkyl halides). It may be noted that some of the absorption peaks recorded for leaf extract and all the nanoparticles remains almost unchanged hinting towards the role of common surface functionalities as capping ligands. We suggest nitro compounds (alkaloids) abundantly present in *C. roseus* leaf as the responsible bioconstituents for reduction of metal ions into nanoparticles. Further, the stability of the nanoparticles could be due to the strong binding of some of the functional groups over the surface of the nanoparticles including carbonyl groups, carboxylic acids, aliphatic amines and alkyl halides.

TEM and SAED measurements

The bright-field TEM images and selected area electron diffraction patterns observed for silver, gold and silver-gold bimetallic nanoparticles are shown in **Fig. 6** and **7**. **Fig. 6a** depicts irregularly shaped, slightly monodispersed silver nanoparticles within the range of 11-26 nm. In case of photosynthesized gold nanoparticles (**Fig.6c**), TEM image has confirmed synthesis of AuNPs, anisotropic in nature showing diverse geometry such as triangles, hexagonals, spheres and rods. The maximum of the gold nanoparticles were reported to be in the spherical shape with mean diameter size 21 nm, while other geometries of gold nanoparticles, particularly triangles were observed well within the range of 25-65 nm. Gold nanotriangles might be nucleated by a process of rapid reduction, assembly and sintering of gold nano spheres at room temperature **[25]**, whereas, in contrast to this, the gradual ripening of silver ions into nanoparticles and its subsequent weak shielding with biomolecules eliminates the possibilities of sintering of smaller silver nanoparticles. This further result shows formation of isotropic, spherical silver nanoparticles rather than silver nanotriangles **[26]**.

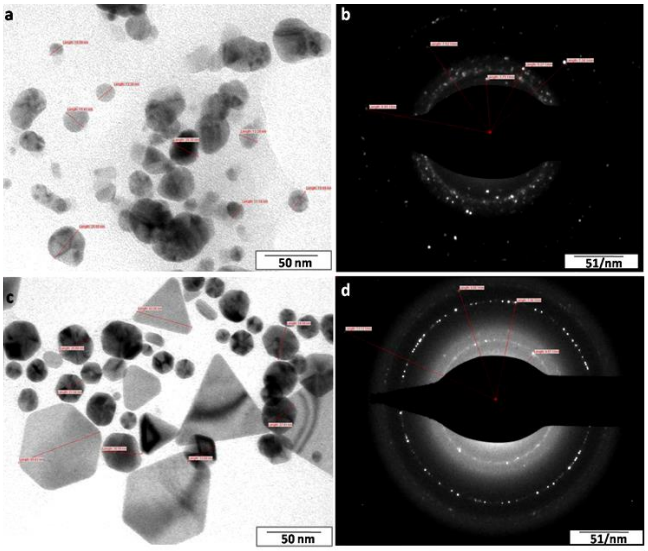

Fig. 6. TEM images observed for (a) AgNPs, (c) AuNPs at 50 nm scales of magnification and SAED pattern recorded for (b) AgNPs and (d) AuNPs at 51/nm scale of magnification.

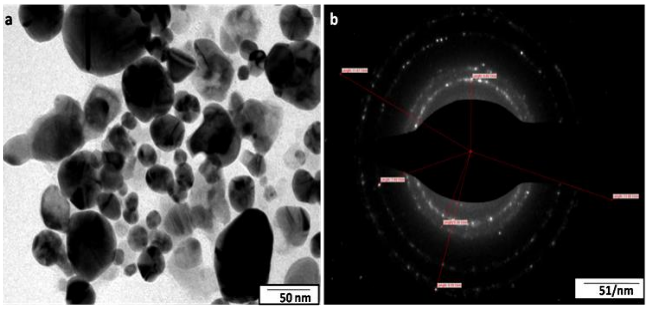

Fig. 7. (a) TEM image and (b) SAED pattern observed for Ag-AuNPs at 50 nm scale of magnification.

Hence, it can be concluded that, protective layering of biomolecules resists formation of anisotropic nanoparticles with diverse geometry. TEM image of the Ag-Au nanospheres is shown in (**Fig. 7a**), with typical diameters of 20–25 nm. TEM images also reveals quite segregated population of nanoparticles which can be attributed to presence of surface capping ligands offered by leaf biomass. Due to the nearly close cell parameters of silver and gold, the crystallographic planes of silver cannot be distinguish from that of gold by the resolution of TEM. However, in a limited manner, difference between contrast of shell and core components allows core-shell differentiation. The uneven coating of gold shell over silver seed can be attributed to the irregular shape of silver nanoparticles. The insignificant increase in diameter of silver seed by auro shell further supports rapid reduction of gold ions over the silver core. Further, unlike the individual gold nanoparticles, the absence of nanoparticles with different morphologies in Ag-Au nanoparticles suspension supports the fact that gold ions have been reduced on silver surface only without nucleating into nanoparticles prior to reaching at silver core.

The SAED patterns of Ag (**Fig. 6b**), Au (**Fig. 6d**) and Ag-Au bimetallic nanoparticles (**Fig. 7B**) further suggest crystalline nature of nanoparticles, which have already confirmed by XRD analysis. The intermittent bright dots arranged in concentric Debye-Sherrer rings can be indexed to the (100), (110), (200), (220) and (311) planes of silver, gold and silver-gold nanoparticles.

Antibacterial and anticandidal assay of silver, gold and silver-gold nanoparticles

The growth inhibitory activity of silver, gold and silver-gold core-shell nanoparticles was assayed against *E.coli*, *P. aeruginosa*, *S. aureus*, *C. guilliermondii*, *C. parapsilosis* and *C.utilis*. The values of zone of inhibition and minimum inhibitory concentrations (MIC) of the NPs against tested organisms are given in **Table 1** and **2**. The more or less equivalent growth inhibitory effect in terms of zone of inhibition was observed for silver and silver-gold nanoparticles against all the tested organisms (**Table 1**).

Table 1. Antibacterial and anticandidal activity of nanoparticles.

Name of the strain	Diameter of Zone of inhibition in mm							
	Cont.	AgNPs	AuNPs	Ab1	AuNPs+ Ab1	Ag-AuNPs	Ab2	Ag-AuNPs+Ab2
E. coli	Nil	11±1	Nil	19±0.5	20±0.5	15±1.1	18	20
P. aeruginosa	Nil	10	Nil	18±0.5	21±0.5	14±1.1	18	20±0.5
S. aureus	Nil	10	Nil	20	23±1	13±1	17±1	20±1
C.guilliermondii	Nil	10	Nil	19	21±1	13	21±0.5	24±1
C. parapsilosis	Nil	10	Nil	26	28	13	27±0.5	30
C.utilis	Nil	10	Nil	26	28	13	28±1	30±1

(Note: Ab, standard antibiotics (chloramphenicol and ketoconazole))
(All values are significant at the 0.05%level of significance)

Table 2. Minimum inhibitory concentration of AgNPs and Ag-AuNPs against bacterial and candidal strains.

Name of the strain	Minimum Inhibitory concentration in μg ml^{-1}	
	AgNPs	Ag-AuNPs
E. coli	10	4
P. aeruginosa	10	4
S. aureus	20	6
C.guilliermondii	15	10
C. parapsilosis	25	20
C.utilis	25	15

All values are significant at the 0.05%level of significance.

However, significant increase in the zone of inhibitions was observed for gold and silver-gold nanoparticles in combination with standard antibiotics. Among the tested bacterial strains, *E.coli* and *P. aeruginosa* were found to be most sensitive to *C. roseus* leaves extract mediated synthesised Ag-NPs and Ag-AuNPs resulting into growth inhibition at concentration of 10 μg ml^{-1} and 4 μg ml^{-1} respectively. Whereas, for *Candida* spp., lowest MIC values were recorded for *C. guilliermondii* (15 and 10 μg ml^{-1} for AgNPs and Ag-AuNPs respectively) followed by *C. utilis* and *C. parapsilosis* (**Table 2**). Further, it is evident from the **table 1** that, the activity of AgNPs was significantly accelerated when surface layered with gold nanoparticles. Though, gold nanopartilces did not show antimicrobial activity, the considerable synergistic antimicrobial effect of gold nanoparticles and standard antibiotic was observed. This fact further supports that, Ag-AuNPs bimetallic nanoparticles exhibit enhanced

antimicrobial properties over their monometallic counterparts due to the synergism between metal variables in core-shell arrangement. Our results are in agreement with the previous report **[16]** where enhanced biofilm inhibition was observed by silver-gold nanoparticles as compared to silver and gold nanoparticles.

The present study deals with the novel method, seed mediated growth technique for the synthesis of core-shell bimetallic silver-gold nanoparticles, employing the leaf extracts of *Catharanthus roseus* Linn. The biosynthesis of gold-silver bimetallic and alloy nanoparticles by various plant materials including leaf exracts of *Swietenia mahogani* **[27]**, *Diopyros kaki* **[28]**, extract of edible mushroom *Volvariella volvacea* **[29]**, cruciferous vegetable extracts **[30]**, etc. have been reported.

In our opinion this is the first report on the rapid phytosynthesis of gold and silver-gold nanoparticles using *C. roseus* leaf extract as biological reducing agent. Moreover, the phytoreduction of silver and gold achieved in this study is free from energy input and without the use of additional stabilizing agents. Seed mediated growth technique relies upon initiation of reduction of seed metal component which further eliminates possibility of pre-reduction interactions between metal ion components having different nobility and miscibility. In general, due to the differences in nobility of gold and silver metal, the simultaneous reduction method leads to first reduction of high noble metal followed by reduction of less noble metal, in this case gold and silver respectively **[31]**. This ultimately leads to the formation of gold (core)- silver (shell) bimetallic nanoparticles or alloys. In contrast to this, the introduction of gold ions to the preformed silver nanoparticles, results into reduction of gold metal ions on nano silver surface forming core-shell nanoparticles rather than alloy. Unlike to independent reduction of gold ions into anisotropic nanoparticles, this method often yields isotropic gold shell over silver nanoseed. From the point of view of nanobiotechnology, this is an innovative approach towards synthesizing advanced nanomaterials with precise control over their structure and surface properties.

Conclusion

The present study reports sequential reduction reaction as a novel approach for biofabrication of silver-gold nanoparticles in core-shell arrangement. Here, the gold ions were reduced and got deposited as a shell over *C. roseus* leaf extract mediated pre synthesized silver nanoparticulate seed. All the three types of nanoparticles including silver, gold and silver-gold bimetallics reveal quite polydispersity as it shows particle size within the range 10-65 nm. The maximum nanoparticles showed spherical morphology, however, gold nanoparticles were observed to be anisotropic in nature possessing distinct morphology such as nano triangles, hexagonals, spheres and rods. Further, these silver-gold bimetallic nanoparticles having core-shell arrangement were evaluated for their antibacterial and anticandidal effect, which showed enhanced antimicrobial bioactivity against *E. coli*, *P. aeruginosa* and *C.guilliermondii* than its monometallic counterparts. Further, the catalytic activity of auro shell was also evident by enhancing the bioactivity of silver nanoseed. The present study provides new possibility of synthesizing predetermined bimetallic core-shell nanoparticles without using stabilizing agents. In future, these core-shell nanoparticles can be used as advanced nanomaterials for catalysis, fuel cell applications and drug delivery purposes.

Acknowledgements

Authors gracefully acknowledge financial support from Department of Science and Technology, New Delhi, India for providing INSPIRE fellowship to pursue this piece of research work. We are also thankful to DST project under “Nano Mission Programme” and to University grand commission, New-Delhi for financial assistance under SAP programme.

Reference

1. Patra, S.; Yang, H. *Bull. Korean Chem. Soc.***2009**, *30*, 1485. **DOI:** 10.5012/bkcs.2009.30.1485
2. Jiang, H-L.; Xu, Q. *J Mater Chem*. **2011**, *21*, 13705. **DOI:** 10.1039/C1JM12020D
3. Leteba, G. M.; Lang, C. I. *Sensors*, **2013**, *13*, 10358. **DOI:** 10.3390/s130810358
4. Liu, T-M.; Yu, J.; Chang, C. A.; Chiou, A.; Chiang, H. K.; Chuang, Y-C.; Wu, C-H.; Hsu, C-H.; Chen, P-A.; Huang, C-C. *Sci Rep*. **2014**, *4*, 5593. **DOI:** 10.1038/srep05593
5. Song, Y.; Liu, K.; Chen, S. *Langmuir*, **2012**, *28*, 17143. **DOI:** 10.1021/la303513x
6. Giorgi, L.; Giorgi, R.; Gagliardi, S.; Serra, A.; Alvisi, M.; Signore, M. A.; Piscopiello, A. *J Nanosci Nanotechnol*. **2011**, *11*, 8804. **DOI:** 10.1166/jnn.2011.3463
7. Toshima., N.; Yonezava, T. *New J. Chem*. **1998**, 1179. **DOI:** 10.1039/A805753B
8. Wang, C.; Chi, M.; Li. D.; Strmcnik, D.; van der Vliet, D.; Wang, G.; Komanicky, V.; Chang, K-C; Pauliks, A.P.; Tripkovic, D.; Pearson, J.; More, K. L.; Markovic, N. M.; Stamenkovic, V. *J. Am. Chem. Soc.* **2011**, *133*, 14396. **DOI:** 10.1021/ja2047655
9. Gumeci, C.; Cearnaigh, D. U.; Casadonte, Jr. D. J.; Korzeniewski, C. *J. Mater. Chem. A*, **2013**, *1*, 2322. **DOI:** 10.1039/C2TA00957A
10. Wanh, H-K.; Yi, C-Y.; Li, T.; Wang, W-J.; Fang, J.; Zhao, J-H.; Shen, W-G. *J Nanomaterials*, **2012**, *2012*, Article ID 453915. **DOI:** 10.1155/2012/453915
11. Byeon, J. H.; Kim, Y-W. *Nanoscale*, **2012**, *4*, 6726. **DOI:** 10.1039/C2NR31609A
12. Zhang, X.; Zhang, G.; Zhang, Z.; Su, Z. *Langmuir*, **2013**, *29*, 6722. **DOI:** 10.1021/la400728k
13. Sheny, D. S.; Mathew, J.; Philip, D. *Spectrochim Acta A. Mol Biomol Spectrosc.* **2011**, *79*, 254. **DOI:** 10.1016/j.saa.2011.02.051.
14. AbdelHamid, A. A.; Al-Ghobashy, M. A.; Fawzy, M.; Mohamed, M.B.; Abdel-Mottaleb, M. M.S.A. *ACS Sustainable Chem. Eng*. **2013**, *1*, 1520. **DOI:** 10.1021/sc4000972
15. Castro-Longoria, E.; Vilchis-Nestor, A. R.; Avalos-Borja, M. *Colloids Surf B. Biointerfaces*. **2011**, *83*, 42. **DOI:** 10.1016/j.colsurfb.2010.10.035
16. Salunke, G. R.; Ghosh, S.; Santosh Kumar, R. J.; Khade, S; Vashisth, P; Kale, T; Chopade, S; Pruthi, V; Kundu, G; Bellare, J. R.; Chopade, B. A. *Int J Nanomed*. **2014**, *9*, 2635. **DOI:** 10.2147/IJN.S59834
17. Shmarakov, I. O.; Mukha, I. P.; Karavan, V. V., Chunikhin, O. Y., Marchenko, M. M.; Smirnova, N. P.; Eremenko, A.M. *Nanomedicine*, **2014**, *1*:*6*. **DOI:** 10.5772/59684
18. Rai, M.; Yadav, A.; Gade, A. Silver nanoparticles as a new generation of antimicrobials. *Biotechnol Adv*. **2008**, *27*, 76. **DOI:** 10.1016/j.biotechadv.2008.09.002
19. Rai, M.; Deshmukh, S.; Ingle, A.; Gupta, I.; Galdiero, S.; Galdiero, M. *Crit. Rev. Microbiol.* **2014a**. **DOI:** 10.3109/1040841X.2013.879849
20. Rai, M.; Kon, K.; Ingle, A.; Duran, N.; Galdiero, S.; Galdiero, M. *Appl. Microbiol Biotechnol*, **2014b**, *98*, 1951. **DOI:** 10.1007/s00253-013-5473-x
21. Bindhu, M. R.; Umadevi, M. *Mater Lett*. **2014**, *120*, 122.

DOI: 10.1016/j.matlet.2014.01.108
22. Mukherjee, P.; Roy, M.; Mandal, B. P.; Dey, G.K.; Mukherjee, P. K.; Ghatak, J.; Tyagi, A. K.; Kale, S. P. *Nanotechnology*, **2008**, *19*,075103.
DOI: 10.1088/0957-4484/19/7/075103
23. Huang, J.; Li, Q.; Sun, D.; Lu, Y.; Su, Y.; Yang, X.; Wang, H.; Wang, Y.; Shao, W.; He, N.; Hong, J.; Chen, C. *Nanotechnology*, **2007**, *18*, 105104.
DOI: 10.1088/0957-4484/18/10/105104
24. Shivshankar, S.; Ahmad, A.; Sastry, M. *Biotechno. Prog*. **2003**, *19*, 1627.
DOI: 10.1021/bp034070w
25. Shivshankar, S.; Rai, A.; Ahmad, A.; Sastry, M. *J. Colloid Interf. Sci*. **2004**, *275*, 496.
DOI: 10.1016/j.jcis.2004.03.003
26. Chandran, S. P.; Chaudhary, M.; Pasricha, R.; Ahmad, A.; Sastry, M. *Biotechnol Prog*. **2006**, *22*, 577.
DOI: 10.1021/bp0501423
27. Mondal, S.; Roy, N.; Laskar, R.A.; Sk, I.; Basu, S.; Mandal, D.; Begum, N. A. *Colloids and Surf. B*, **2011**, *82*, 497.
DOI: 10.1016/j.colsurfb.2010.10.007
28. Song, T.; Kim, B. *Korean J Chem Eng*. **2008**, *25*, 808.
DOI: 10.1007/s11814-008-0133-z
29. Philip, D. *Spectrochim. Acta Part A*, **2009**, *73*, 374.
DOI: 10.1016/j.saa.2009.02.037
30. Jacob, J.; Mukherjee, T.; Kapoor, S. *Mater Sci Eng C*, **2012**, *32*, 1827.
DOI: 10.1016/j.msec.2012.04.072
31. Liu, X.; Wang, D.; Li, Y. *Nano Today*, **2012**, *7*, 448.
DOI: 10.1016/j.nantod.2012.08.003

